Filter Design to Address Range Sidelobe Modulation in Transmit-Encoded Radar-Embedded Communications

Cenk Sahin[1], Justin G. Metcalf[1], and Shannon D. Blunt[2]
[1] Sensors Directorate, Air Force Research Laboratory, Wright-Patterson Air Force Base, OH
[2] Department of Electrical Engineering & Computer Science, University of Kansas, Lawrence, KS

***Abstract*—In a companion paper a continuous phase modulation (CPM) based approach has been introduced to embed information sequences into physical radar emissions, yielding spectrally-efficient constant-envelope waveforms. In addition, the CPM-based approach enables direct control of the degree of range sidelobe modulation (RSM), which occurs due to the changing waveform structure during the coherent processing interval (CPI), by trading off bit error rate (BER) and/or data throughput. When not properly addressed, RSM translates to residual clutter in the range-Doppler response, and hence degraded target visibility.**

Here receive filter design to mitigate RSM is addressed. The objective for such filters is to produce pulse compression responses that are similar despite the pulse-to-pulse change in waveforms. Three different filter designs are proposed and compared by simulation, where it is found that coherence can be enhanced (and thus RSM reduced) at the expense of higher range sidelobes.

I. Introduction

While the radio spectrum remains a limited resource, the demand by commercial communication applications has been exponentially increasing [1]. As a result, radar sensing applications that must already operate in congested and contested environments are struggling to maintain legacy capabilities. Accordingly, ongoing research is focused on developing methods to share spectrum between multiple functions such as radar and communications [2]. Radar/communication spectrum sharing necessitates the use of some manner of waveform diversity [3]–[6], which involves the exploitation of the available time, frequency, coding, spatial, and polarization degrees-of-freedom. The waveform diversity approach most relevant to the proposed multi-function radar/communication formulation is coding diversity, where distinct radar waveforms are used as communication symbols and the set of radar waveforms serves as a communication symbol alphabet [7]–[12].

When radar waveforms are used as communication symbols, the radar emission changes on a pulse-to-pulse basis (referred to as *pulse agility or waveform agility*). The primary issue with varying the radar waveform during a coherent processing interval (CPI) is the clutter *range sidelobe modulation* (RSM) [7], [13], [14] that arises because the pulse compression of different waveforms leads to different sidelobe structures. When Doppler processing is performed on the CPI of pulsed echoes, the presence of RSM induces a partial loss of coherency, resulting in residual clutter after cancellation, and hence reduced target visibility. It follows that RSM is a very important design consideration for this manner of multi-function radar/communication systems.

Maintaining both power efficiency and spectral efficiency is of great interest for radar systems to maximize "energy on target" and to limit the spectral roll-off for sufficient spectral containment. Accordingly, a CPM-based framework was recently developed in [15] to implement polyphase radar codes as physically realizable frequency-modulated (FM) waveforms, denoted by polyphase-coded FM (PCFM). The continuous phase feature of such CPM-based signals leads to high spectral efficiency, while the constant envelope feature allows the transmitter power amplifier to be operated in saturation such that available power is efficiently converted into radiated power. In the companion paper [12] a new approach to embed communications into radar is formulated in which information-bearing sequences are modulated with CPM and phase-attached to a PCFM-implemented *fixed* radar waveform. The result is a CPM-based communication-embedded radar waveform for each pulse, thus ensuring high power and spectral efficiency. More importantly, adjustable implementation parameters provide control of the degree of RSM by trading off bit error rate (BER) and/or data throughput.

Here receive filter design is addressed for the purpose of reducing RSM within this CPM-based communication-embedded radar framework. The two main objectives for receive filter design in this context are 1) to maximize the similarity of the filter responses across the set of different information-bearing waveforms and 2) to reduce the range sidelobes. The design methods focus on realization of a desired common filter response, rather than optimization of individual receive filters. The inherent commonality among the radar/communication waveforms stemming from the common phase component, namely the base radar waveform, is exploited. With the matched filter (MF) approach, the MF

This research was performed while Cenk Sahin held an NRC Research Associateship award at the Air Force Research Laboratory, Wright-Patterson AFB, OH. This work was supported in part by the Air Force Research Laboratory - Sensors Directorate, and by a subcontract with Matrix Research, Inc. for research sponsored by the Air Force Research Laboratory under Prime Contract #FA8650-14-D-1722.

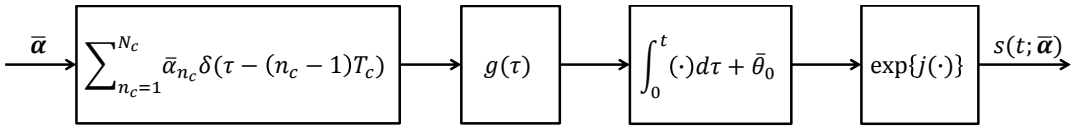

Fig. 1. Block diagram of CPM-based PCFM implementation for radar [15].

output of the base radar waveform is used as the desired filter response. With the mismatch filter (MMF) approach, the desired filter response consists of a mainlobe identical to that of the MF output of the base radar waveform with zeros elsewhere. Finally, a cascaded filter approach is proposed in which two receive filters, based on the MF and MMF approaches are used in series, where the first filter enhances similarity across the pulse compression responses while the second filter reduces the range sidelobes.

Filter design to mitigate RSM for a given set of waveforms has been previously addressed [7], [8], [16]–[19]. The joint least squares (JLS) approach introduced in [7] is only suitable for a small number of distinct waveforms ($\sim 2-4$) because the sidelobe performance degrades as the number of waveforms increases. The closed form solution for the JLS approach derived in [8] for moving target indication (MTI) is likewise only applicable to small a number of distinct waveforms. Neither of these approaches are suitable for the CPM-based communication-embedded radar because the number of distinct waveforms is exponential with the time-bandwidth product. In [16]–[19] joint range-Doppler processing was considered for pulse-agile emissions, with attendant increases in computational cost. Finally, if the individual pulse-agile waveforms are themselves optimized to provide low sidelobes (see [13]), then simpler mismatched receiver filtering can be employed. Of course, the present communication-embedded radar waveforms are not expected to individually possess low sidelobes.

II. System Model

Consider the polyphase radar code $\overline{\boldsymbol{\theta}} = [\overline{\theta}_0, \cdots, \overline{\theta}_{N_c}]$, where N_c denotes the number of chips per pulse and $|\overline{\theta}_{n_c}| \leq \pi$ for all $n_c = 0, \cdots, N_c$ [15], [20]. The CPM-based PCFM implementation is shown in Fig. 1. The sequence $\overline{\boldsymbol{\alpha}} = [\overline{\alpha}_1, \cdots, \overline{\alpha}_{N_c}]$, where $|\overline{\alpha}_{n_c}| \leq \pi$ for all $n_c = 1, \cdots, N_c$, denotes the phase changes between successive chips of $\overline{\boldsymbol{\theta}}$. The overline notation $\overline{(\cdot)}$ is used with $\overline{\boldsymbol{\theta}}$ and $\overline{\boldsymbol{\alpha}}$ to emphasize that both are fixed sequences (do not change from pulse to pulse). The length-N_c train of impulses, with the n_c-th impulse scaled by $\overline{\alpha}_{n_c}$, is convolved with shaping filter $g(t)$ and then integrated to produce the continuous phase of the radar waveform

$$\psi(t;\overline{\boldsymbol{\alpha}}) = \int_0^t g(\tau) * \left[\sum_{n_c=1}^{N_c} \overline{\alpha}_{n_c}\delta(\tau-(n_c-1)T_c)\right] d\tau + \overline{\theta}_0, \tag{1}$$

where T_c is the time duration of the chip interval, $*$ denotes convolution, and $\overline{\theta}_0$ is the initial phase value. The shaping filter $g(t)$ has time support $[0, T_c]$, and the area under $g(t)$ is 1. The resulting PCFM radar waveform of time duration $T = N_c T_c$, referred to as the *base radar waveform*, is

$$s(t;\overline{\boldsymbol{\alpha}}) = \sqrt{P_t} e^{j\psi(t;\overline{\boldsymbol{\alpha}})}, \tag{2}$$

where P_t is the transmit power.

Now consider the communication symbol sequence $\boldsymbol{\beta} = [\beta_1, \cdots, \beta_{N_s}]$ drawn from the M-ary symbol alphabet $\{\pm 1, \pm 3, \cdots, \pm(M-1)\}$ where N_s is the number of symbols per pulse and $M = 2^m$, with m the number of bits/symbol. The symbol sequence $\boldsymbol{\beta}$ is modulated as a CPM waveform with symbol interval T_s and the communication shaping filter $g_c(t)$, resulting in the signal phase $\phi(t;\boldsymbol{\beta})$ given by [21]

$$\phi(t;\boldsymbol{\beta}) = p\pi \int_0^t g_c(\tau) * \left[\sum_{n_s=1}^{N_s} \beta_{n_s}\delta(\tau-(n_s-1)T_s)\right] d\tau, \tag{3}$$

where p is a rational number referred to as the *modulation index*. The communication shaping filter $g_c(t)$ has time duration LT_s with L a positive integer, and the area under $g_c(t)$ is also 1. Here we focus on the full-response CPM where $L = 1$. The signal phase $\phi(t;\boldsymbol{\beta})$ has the same duration (pulsewidth $T = N_c T_c$) as the base radar waveform. It follows that for a given base radar waveform, i.e. fixed T, the symbol interval $T_s = \frac{T}{N_s}$ can be decreased/increased to achieve an increased/decreased symbol rate.

To transmit the communication sequence $\boldsymbol{\beta}$ within the radar emission, $\phi(t;\boldsymbol{\beta})$ is phase-attached to the base radar waveform $s(t;\overline{\boldsymbol{\alpha}})$, which results in the information-bearing continuous-phase radar/communication waveform

$$\tilde{s}(t;\overline{\boldsymbol{\alpha}},\boldsymbol{\beta}) = \sqrt{P_t} e^{j(\psi(t;\overline{\boldsymbol{\alpha}})+\phi(t;\boldsymbol{\beta}))}. \tag{4}$$

We emphasize that $\boldsymbol{\beta}$ is a random sequence that changes on a pulse-to-pulse basis. The base radar waveform $s(t;\overline{\boldsymbol{\alpha}})$ maintains a degree of commonality among the set of changing waveforms in the CPI while the differences are uniquely specified by the modulation index p, the communication symbol alphabet size M, and the symbol duration T_s. In particular, the radar/communication waveforms become more alike, and thus RSM is reduced, as p or M is decreased and T_s is increased [12]. From a communication performance perspective, a smaller p translates to higher BER, while a smaller M or larger T_s translates to lower data throughput [12].

III. Filter Design Methods

With this CPM-based communication-embedded radar framework, the severity of RSM can be mitigated at the expense of increased BER or decreased data throughput. Here it is demonstrated that, for fixed system parameters, RSM can be mitigated by the design of appropriate receive filters, i.e. a

unique receive filter for each communication-embedded radar waveform. As a result, radar performance can be enhanced without sacrificing communication performance.

Ideally, the objective in receive filter design would be to find filters $h_i(t), i = 1, \cdots, 2^{mN_s}$, satisfying (for all i) [7]

$$s_i(t) * h_i(t) = y(t), \tag{5}$$

where $s_i(t)$ is the i-th communication-embedded radar waveform and $y(t)$ is the common filter response, preferably with low range sidelobes. If the condition in (5) could be satisfied, RSM would not occur. However, as discussed in [7], the condition in (5) cannot be achieved with finite-length filters for more than two different waveforms. Generalizing [7], the discrete-time equivalent of the filtering operation in (5), for filter length $\widetilde{N}$ (samples), can be expressed by the matrix equation

$$\mathbf{A}_i \mathbf{h}_i = \mathbf{y}, \tag{6}$$

where $\mathbf{A}_i$ is the $(\widetilde{N} + N_c K - 1) \times \widetilde{N}$ *delay-shift matrix* for the i-th waveform $s_i(t)$ given by

$$\mathbf{A}_i = \begin{bmatrix} s_{i,1} & 0 & \cdots & 0 \\ \vdots & s_{i,1} & & \vdots \\ s_{i,N_c K} & \vdots & \ddots & 0 \\ 0 & s_{i,N_c K} & & s_{i,1} \\ \vdots & & \ddots & \vdots \\ 0 & \cdots & & s_{i,N_c K} \end{bmatrix}, \tag{7}$$

and $\mathbf{s}_i = [s_{i,1}, \cdots, s_{i,N_c K}]^T$, $\mathbf{h}_i = [h_{i,1}, \cdots, h_{i,\widetilde{N}}]^T$ and $\mathbf{y} = [y_1, \cdots, y_{\widetilde{N}+N_c K-1}]^T$ are the discretized versions of $s_i(t)$, $h_i(t)$ and $y(t)$, respectively. These discretized versions are sampled at a rate of K samples/chip to ensure sufficient "oversampling" relative to 3-dB bandwidth (nominal sampling would correspond to $K = 1$). While (6) cannot be satisfied for all i, the objective is to minimize the (average) incoherence among the filter responses. Accordingly, the *mismatch metric* $\Delta_{\text{MM}} = \mathbb{E}[\Delta_{i,j}]$ is proposed, where $\mathbb{E}[\cdot]$ is the expectation operator and $\Delta_{i,j}, i \neq j$, is defined as

$$\Delta_{i,j} \triangleq \frac{||\mathbf{A}_i \widehat{\mathbf{h}}_i - \mathbf{A}_j \widehat{\mathbf{h}}_j||^2}{\mathbb{E}\left[||\mathbf{A}_i \widehat{\mathbf{h}}_i||^2\right]}, \tag{8}$$

for $\widehat{\mathbf{h}}_i$ the estimate of the i-th filter. The mismatch metric quantifies the ratio of the pairwise *incoherent* filter response energy to the average filter response energy.

The least-squares (LS) mismatched filter solution [7], [15], [22], [23] for a given discretized waveform $\mathbf{s}_i$ sets $\mathbf{y} = \mathbf{e}$ in (6), yielding

$$\widehat{\mathbf{h}}_{\text{LS},i} = \left(\mathbf{A}_i^H \mathbf{A}_i + \delta \mathbf{I}\right)^{-1} \mathbf{A}_i^H \mathbf{e}, \tag{9}$$

where $\mathbf{A}_i^H$ denotes the Hermitian transpose of $\mathbf{A}_i$, $\mathbf{e} = [0, ..., 0, 1, 0, ..., 0]^T$ is an elementary vector with the non-zero element corresponding to the match point, and the diagonal loading term $\delta \mathbf{I}$ may be invoked to prevent ill-conditioning. While this filter can minimize the range sidelobes for a single waveform, it does not address the problem of sidelobe incoherence across a set of different waveforms. In contrast, we consider a modification to (9) in the spirit of [7] in which the elementary vector $\mathbf{e}$ that forces an impulse-like LS filter response is generalized to the vector $\mathbf{y}$ that serves as a desired common filter response. This approach provides a framework with which to explore various trade-offs such as the coherence among the filter responses and the (average) peak-to-sidelobe ratio of the filter responses. For a given $\mathbf{y}$ and a discretized $\mathbf{s}_i$, this "common response" LS filter is

$$\widehat{\mathbf{h}}_i = \left(\mathbf{A}_i^H \mathbf{A}_i + \delta \mathbf{I}\right)^{-1} \mathbf{A}_i^H \mathbf{y}. \tag{10}$$

Note that the receive filters $\{\widehat{\mathbf{h}}_i\}$, and thus the mismatch metric, are uniquely specified by the common response $\mathbf{y}$.

An additional useful metric for mismatched filter design is the SNR loss due to mismatch [24]. For this formulation in which the waveform, and thus the filter, changes for each pulse, the SNR loss is computed as the expected value of the ratio of the peak SNR at the output of the matched filter (MF) to the peak SNR at the output of the receive filter, or

$$\text{SNR Loss (dB)} = 10 \log_{10} \frac{P_{\text{peak,MF}}/||\mathbf{s}_i||^2}{\mathbb{E}\left[P_{\text{peak},i}/||\widehat{\mathbf{h}}_i||^2\right]}. \tag{11}$$

In (11), $P_{\text{peak,MF}}$ is the peak power at the output of the MF, which is a constant and given by $P_{\text{peak,MF}} = P_t (N_c K)^2$ for all waveforms. Likewise $P_{\text{peak},i}$ is the peak power at the output of the i-th receive filter. Note that the norm of the MF for waveform i, denoted by $||\mathbf{s}_i||$, is a constant for all i. In the following sections we examine the impact of the selection of the desired common response $\mathbf{y}$.

A. Matched Filter Common Response

Embedding communication symbols into radar emissions in the system under consideration causes small phase perturbations *relative* to the phase trajectory of the base radar waveform. Accordingly, the MF output of each waveform is similar to the MF output of the base radar waveform $s_{\text{r}}(t)$, with the degree of similarity increasing with decreasing p. In addition, it intuitively makes sense to choose a common filter response that is consistent with that of the base radar waveform. Hence, the MF output of the base radar waveform can be used to establish the common response via

$$\mathbf{y}_{\text{MF}} = \mathbf{A}_{\text{r}} \, \mathbf{s}_{\text{r,MF}}, \tag{12}$$

where $\mathbf{A}_{\text{r}}$ is the delay-shift matrix of the base radar waveform like (7), and $\mathbf{s}_{\text{r,MF}} = [s_{\text{r},NK}^*, \cdots, s_{\text{r},1}^*]^T$ is the complex conjugated and time-reversed discretized version of the base radar waveform $s_{\text{r}}(t)$. Then, for each waveform $\mathbf{s}_i$, the filter $\widehat{\mathbf{h}}_i$ is computed from (10) with $\mathbf{y} = \mathbf{y}_{\text{MF}}$. Note that the filter $\widehat{\mathbf{h}}_i$ is not constrained to have the same length as the MF. When the length of $\widehat{\mathbf{h}}_i$ is greater than NK, the common response $\mathbf{y}_{\text{MF}}$ is zero-padded accordingly.

As an example, a PCFM-implemented linear FM (LFM) chirp [15] is used as the base radar waveform with parameters

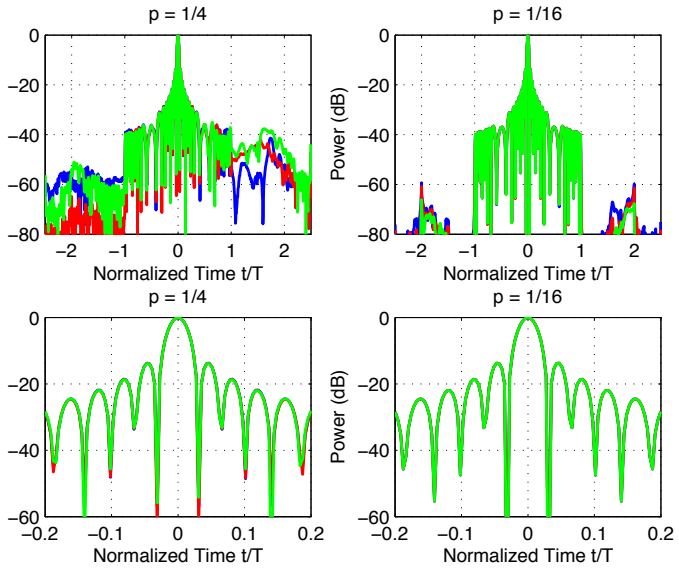

Fig. 2. Filter responses using (10) and (12) of three randomly generated waveforms (top) and close-up view (bottom) for $p = \frac{1}{4}$ and $p = \frac{1}{16}$.

$N_c = 32$ chips/pulse (so the time-bandwidth product is likewise 32), and $K = 8$ samples/chip. The receive filter length is $\widetilde{N} = 1024$ samples (4 times the discretized length of the waveform). The communication symbols are binary with $N_s = 32$ symbols/pulse. In Fig. 2 the filter response powers using (10) and (12) are plotted for three randomly generated communication sequences embedded into the base radar waveform for modulation indices $p = \frac{1}{4}$ and $\frac{1}{16}$. The filter response (top) and a close-up version (bottom) are shown. Diagonal loading in (10) is not used, so $\delta = 0$. The filter responses in Fig. 2 exhibit sufficient coherence for both p values with the $p = \frac{1}{16}$ case being superior. The resulting mismatch metric from (8) is shown in Table I (first row) for modulation index values $p = \frac{1}{2}, \frac{1}{4}, \frac{1}{8}$ and $\frac{1}{16}$. The mismatch metric value decreases with decreasing p as expected. If the number of symbols/pulse N_s is reduced, the filter responses will match even more closely and the mismatch metric values will further decrease. Per Table II (first row), the SNR loss likewise decreases with decreasing p.

B. Mismatch Filter Common Response

Now consider the case in which the common response is itself constructed from a mismatch filter formulation via

$$\mathbf{y}_{\text{MMF}} = \mathbf{A}_{\text{r}} \left[\left(\mathbf{A}_{\text{r}}^H \mathbf{A}_{\text{r}} + \delta \mathbf{I} \right)^{-1} \mathbf{A}_{\text{r}}^H \mathbf{y}_{\text{MF,main}} \right], \qquad (13)$$

where

$$\mathbf{y}_{\text{MF,main}} = [0, \cdots, 0, y_{\text{MF},-K+NK}, \cdots, y_{\text{MF},K+NK}, 0, \cdots, 0]^T, \qquad (14)$$

in which the non-zero terms comprise only the mainlobe of the MF response $\mathbf{y}_{\text{MF}}$. In a similar manner to the spectrum-shaping LS formulation in [14], the objective of this approach is to trade the prospect of enhanced range resolution (i.e. we wish to maintain nominal resolution [25]) for a less constrained LS problem.

TABLE I
MISMATCH METRIC

	$p = \frac{1}{2}$	$p = \frac{1}{4}$	$p = \frac{1}{8}$	$p = \frac{1}{16}$
MF via (10), (12)	3×10^{-2}	6×10^{-3}	4×10^{-5}	2×10^{-6}
MMF via (10), (13)	4×10^{-2}	7×10^{-3}	5×10^{-4}	2×10^{-4}
Cascade via (15), (17)	6×10^{-2}	1×10^{-2}	3×10^{-4}	4×10^{-5}
Standard LS via (9)	1×10^{-1}	8×10^{-2}	1×10^{-2}	3×10^{-3}

TABLE II
SNR LOSS

	$p = \frac{1}{2}$	$p = \frac{1}{4}$	$p = \frac{1}{8}$	$p = \frac{1}{16}$
MF via (10), (12)	6.9 dB	5.4 dB	1.3 dB	0.3 dB
MMF via (10), (13)	7.9 dB	6.9 dB	5.4 dB	4.5 dB
Cascade via (15), (17)	6.0 dB	4.7 dB	1.6 dB	0.7 dB
Standard LS via (9)	4.0 dB	3.4 dB	1.5 dB	0.8 dB

Using the same parameters as the previous example, the filter responses using (13) and (10) for three randomly generated waveforms are shown in Fig. 3. Diagonal loading is not used because it has been observed to increase the mismatch metric of (8). The filter outputs match more closely as the modulation index decreases. The range sidelobes are also much lower than those obtained with the previous approach. Per Tables I and II (second row) the SNR loss values and mismatch metric values are both greater than those obtained for the MF approach. The difference between the two approaches in terms of the SNR loss and mismatch metric is more pronounced for the modulation index values $p = \frac{1}{8}$ and $p = \frac{1}{16}$. The numerical results suggest that the range sidelobes can be reduced at the expense of an increased mismatch metric (i.e. increased range sidelobe modulation) and SNR loss.

For completeness, Tables I and II (bottom row) also provide the SNR loss and mismatch metric for the case in which standard LS mismatched filter from (9) is used. When the standard mismatched filter is used, the "beamspoiling" approach described in [20], [23] is also employed to prevent an undesirable super-resolution condition [25]. Diagonal loading is used with $\delta = 0.1$, which minimizes the mismatch metric. It is observed in Table I that the mismatch metric values are greater than those obtained for the MMF approach, especially for $p = \frac{1}{8}$ and $p = \frac{1}{16}$ the mismatch metric values are significantly greater. According to Table II the SNR loss values are lower than those obtained for the MMF approach while they are higher/lower than those obtained for the MF approach for $p = \frac{1}{8}$ and $\frac{1}{16}$ / $p = \frac{1}{2}$ and $\frac{1}{4}$.

C. Cascade of Matched Filter and Mismatch Filter

As previously stated, the two goals in pulse-agile receive filter design are to maximize the similarity among the filter responses and to minimize the range sidelobes. Now consider the case where these two goals are *decoupled* by a cascade of two receive filters in series. The first filter (MF approach) improves the similarity of the filter responses while the second

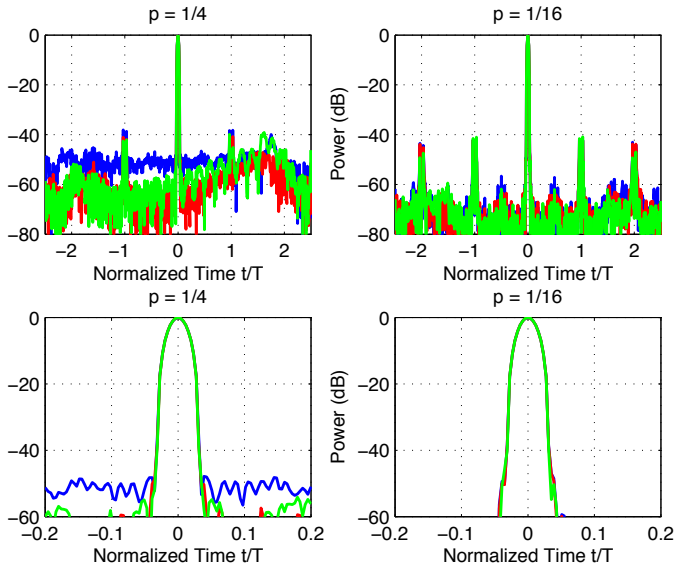

Fig. 3. Filter responses using (13) and (10) for three randomly generated waveforms (top) and close-up view (bottom) for $p = \frac{1}{4}$ and $p = \frac{1}{16}$.

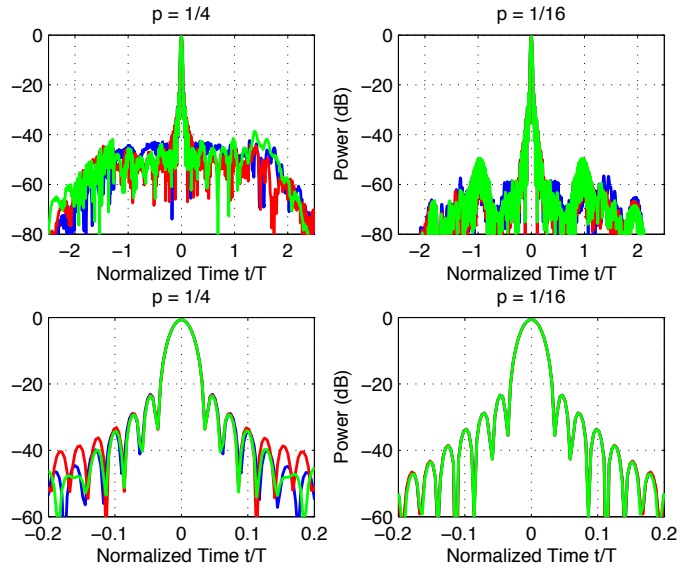

Fig. 4. Filter responses using (15) and (17) for three randomly generated waveforms (top) and close-up view (bottom) for $p = \frac{1}{4}$ and $p = \frac{1}{16}$.

filter (MMF approach) subsequently reduces the sidelobes. The motivation here is driven by the success of the MF approach using (10) and (12) to produce good similarity among the filter responses.

The first filter has length-$\widetilde{N}_1$ and is computed for each waveform $\mathbf{s}_i$ from (10) with the MF common response $\mathbf{y}_{\text{MF}}$ from (12) as

$$\widehat{\mathbf{h}}_{\text{CMF},i} = \left(\mathbf{A}_i^H \mathbf{A}_i + \delta \mathbf{I}\right)^{-1} \mathbf{A}_i^H \mathbf{y}_{\text{MF}}, \tag{15}$$

where $\mathbf{A}_i$ is $(\widetilde{N}_1 + N_c K - 1) \times \widetilde{N}_1$. The output of the first filter is the length-$(\widetilde{N}_1 + N_c K - 1)$ vector

$$\mathbf{r}_i = \mathbf{A}_i \, \widehat{\mathbf{h}}_{\text{CMF},i}. \tag{16}$$

Using $\mathbf{r}_i$, now construct another delay-shift matrix similar to (7) denoted as $\mathbf{B}_i$, which has dimensionality $(\widetilde{N}_2 + \widetilde{N}_1 + N_c K - 2) \times \widetilde{N}_2$ for $\widetilde{N}_2$ the length of the second filter. The second filter is then computed based on the MMF approach from (10) as

$$\widehat{\mathbf{h}}_{\text{CMMF},i} = \left(\mathbf{B}_i^H \mathbf{B}_i + \delta \mathbf{I}\right)^{-1} \mathbf{B}_i^H \mathbf{y}_{\text{CMMF}}, \tag{17}$$

where the common filter response $\mathbf{y}_{\text{CMMF}}$ is

$$\mathbf{y}_{\text{CMMF}} = \mathbf{B}_{\text{r}} \left[\left(\mathbf{B}_{\text{r}}^H \mathbf{B}_{\text{r}} + \delta \mathbf{I}\right)^{-1} \mathbf{B}_{\text{r}}^H \mathbf{y}_{\text{MF,main}}\right], \tag{18}$$

$\mathbf{y}_{\text{MF,main}}$ is defined in (14), and $\mathbf{B}_{\text{r}}$ is the delay-shift matrix constructed from $\mathbf{y}_{\text{MF}}$ in (12) (the output of the first filter for the base radar waveform). Given that the output of the first filter for each waveform satisfies $\mathbf{r}_i \approx \mathbf{y}_{\text{MF}}$, the design of the second common response can be based directly on $\mathbf{y}_{\text{MF}}$.

The cascade filtering approach for waveform $\mathbf{s}_i$ can be represented by a single filter $\widehat{\mathbf{h}}_{\text{C},i}$ of length $\widetilde{N}_1 + \widetilde{N}_2 - 1$, which is simply the convolution of $\widehat{\mathbf{h}}_{\text{CMF},i}$ and $\widehat{\mathbf{h}}_{\text{CMMF},i}$. A fair comparison between this cascade approach and the previously described approaches requires the (total) filter lengths to be the same; accordingly, we set $\widetilde{N} = \widetilde{N}_1 + \widetilde{N}_2 - 1$. In addition, each filter is constrained to be no shorter that the length of its input so $\widetilde{N}_1 \geq NK$ and $\widetilde{N}_2 \geq \widetilde{N}_1 + NK - 1$, which imply $(\widetilde{N} - NK)/2 + 1 \geq \widetilde{N}_1 \geq NK$.

The filter lengths used for simulation results are $\widetilde{N}_1 = 384$ and $\widetilde{N}_2 = 641$. Diagonal loading of $\delta = 0.25$ is used in both (17) and (18) to reduce the mismatch metric value. Diagonal loading also raises the range sidelobe level at the output of the second filter, so the value $\delta = 0.25$ is chosen judiciously to balance between the mismatch metric performance and the range sidelobe level. All other parameters are the same as those used previously. The filter responses using (15) and (17) for three randomly generated waveforms are shown in Fig. 4. The range sidelobes are reduced compared to the MF approach, while they are higher than those obtained with the MMF approach. According to Table I (third row) the mismatch metric values observed are lower/higher than they are with the MMF/MF approach for $p = \frac{1}{8}$ and $p = \frac{1}{16}$. It can therefore be concluded that the cascade filtering approach provides a further trade off between coherence among the filter responses and reduced range sidelobes. Per Table II (third row) the SNR loss values for the cascade approach are smaller than/comparable to those observed for the MMF/MF approach.

IV. Conclusions

Receive filter design to mitigate RSM is addressed for the CPM-based communication-embedded radar framework introduced in a companion paper. Design methods focus on the realization of a common filter response and exploit the inherent commonality among the radar/communication waveforms. The simulation results show that coherence across pulse compression responses of different waveforms can be enhanced, and thus RSM reduced, as a trade-off for higher range sidelobes.

REFERENCES

[1] H. Griffiths, L. Cohen, S. Watts, E. Mokole, C. Baker, M. Wicks, and S. D. Blunt, "Radar spectrum engineering and management: Technical and regulatory issues," *Proceedings of the IEEE*, vol. 103, pp. 85–102, Jan 2015.

[2] Strategic Technology Office and Defense Advanced Research Projects Agency, *Shared Spectrum Access for Radar and Communications (SSPARC)*. [Online]. Available: http://www.darpa.mil/program/shared-spectrum-access-for-radar-and-communications, accessed Jan. 2016.

[3] M. Wicks, E. Mokole, S. Blunt, R. Schneible, and V. Amuso, eds., *Principles of Waveform Diversity and Design*. Raleigh, NC: SciTech Publishing, 2010.

[4] S. Pillai, K. Y. Li, and B. Himed, *Waveform Diversity: Theory & Applications*. McGraw-Hill, 2011.

[5] F. Gini, A. D. Maio, and L. K. Patton, eds., *Waveform Design and Diversity for Advanced Radar Systems*. Croydon, UK: Institution of Engineering and Technology, 2012.

[6] S. D. Blunt and E. L. Mokole, "Overview of radar waveform diversity," *IEEE Aerospace and Electronic Systems Magazine*, vol. 31, pp. 2–42, Nov. 2016.

[7] S. D. Blunt, M. R. Cook, and J. Stiles, "Embedding information into radar emissions via waveform implementation," *International Waveform Diversity and Design Conference*, pp. 195–199, Aug. 2010.

[8] A. C. O'Connor, J. M. Kantor, and J. Jakabosky, "Joint equalization filters that mitigate waveform-diversity modulation of clutter," *IEEE Radar Conference*, May 2016.

[9] L. Reichardt, C. Sturm, F. Grunhaupt, and T. Zwick, "Demonstrating the use of the IEEE 802.11P car-to-car communication standard for automotive radar," *6th European Conference on Antennas and Propagation*, pp. 1576–1580, Mar. 2012.

[10] X. Chen, X. Wang, S. Xu, and J. Zhang, "A novel radar waveform compatible with communication," *International Conference on Computational Problem-Solving*, pp. 177–181, Oct. 2011.

[11] M. J. Nowak, Z. Zhang, Y. Qu, D. A. Dessources, M. Wicks, and Z. Wu, "Co-designed radar-communication using linear frequency modulation waveform," *IEEE Military Communications Conference*, pp. 918–923, Nov. 2016.

[12] C. Sahin, J. Jakabosky, P. M. McCormick, J. G. Metcalf, and S. D. Blunt, "A novel approach for embedding communication symbols into physical radar waveforms," *IEEE Radar Conference*, Seattle, WA, May 2017.

[13] M. R. Cook, S. D. Blunt, and J. Jakabosky, "Optimization of waveform diversity and performance for pulse-agile radar," in *Proceedings of the 2011 IEEE Radar Conference*, pp. 812–817, May 2011.

[14] J. Jakabosky, S. D. Blunt, and B. Himed, "Spectral-shape optimized FM noise radar for pulse agility," *IEEE Radar Conference*, May 2016.

[15] S. D. Blunt, M. R. Cook, J. Jakabosky, J. De Graaf, and E. Perrins, "Polyphase-coded FM (PCFM) radar waveforms, part I: implementation," *IEEE Transactions on Aerospace and Electronic Systems*, vol. 50, pp. 2218–2229, July 2014.

[16] D. Scholnik, "Range-ambigious clutter suppression with pulse-diverse waveforms," *IEEE Radar Conference*, pp. 336–341, May 2011.

[17] T. Higgins, S. D. Blunt, and A. K. Shackelford, "Time-range adaptive processing for pulse agile radar," *International Waveform Diversity and Design Conference*, pp. 115–120, Aug. 2010.

[18] T. Higgins, K. Gerlach, A. K. Shackelford, and S. D. Blunt, "Aspects of non-identical multiple pulse compression," *IEEE Radar Conference*, pp. 895–900, May 2011.

[19] A. C. O'Connor, J. M. Kantor, and J. Jakabosky, "Space-time adaptive mismatch processing," *IEEE Radar Conference*, May 2016.

[20] S. D. Blunt, J. Jakabosky, M. R. Cook, J. Stiles, S. Seguin, and E. Mokole, "Polyphase-coded FM (PCFM) radar waveforms, part II: optimization," *IEEE Transactions on Aerospace and Electronic Systems*, vol. 50, pp. 2230–2241, July 2014.

[21] J. B. Anderson, T. Aulin, and C.-E. Sundberg, *Digital Phase Modulation*. New York: Plenum Press, 1986.

[22] M. H. Ackroyd and F. Ghani, "Optimum mismatched filters for sidelobe suppression," *IEEE Transactions on Aerospace and Electronic Systems*, vol. AES-9, pp. 214–218, Mar. 1973.

[23] D. Henke, P. M. McCormick, S. D. Blunt, and T. Higgins, "Practical aspects of optimal mismatch filtering and adaptive pulse compression for fm waveforms," *IEEE Radar Conference*, pp. 1149–1155, May 2015.

[24] M. A. Richards, J. A. Scheer, and W. Holm, *Principles of Modern Radar, Vol. I: Basic Principles*. Raleigh, NC: SciTech Publishing, 2010.

[25] S. D. Blunt, K. Gerlach, and T. Higgins, "Aspects of radar range super-resolution," *IEEE Radar Conference*, pp. 683–687, Apr. 2007.